Room-temperature electric control of exchange bias effect in $CoO_{1-\delta}$/Co films using $Pb(Mg_{1/3}Nb_{2/3})_{0.7}Ti_{0.3}O_3$ (110) substrates*

Xin Wen(闻馨)[1], Rui Wu(吴锐)[1,†], Wen-Yun Yang(杨文云)[1,2,3], Chang-Sheng Wang(王常生)[1,2,3], Shun-Quan Liu(刘顺荃)[1,2,3], Jing-Zhi Han(韩景智)[1,2,3], and Jin-Bo Yang(杨金波)[1,2,3]

[1] *State Key Laboratory for Mesoscopic Physics and School of Physics, Peking University, Beijing* 100871, *China*
[2] *Beijing Key Laboratory for Magnetoelectric Materials and Devices, Beijing* 100871, *China*
[3] *Collaborative Innovation Center of Quantum Matter, Beijing* 100871, *China*

(Received 8 June 2020; revised manuscript received 3 July 2020; accepted manuscript online 15 July 2020)

Significant electric control of exchange bias effect in a simple $CoO_{1-\delta}$/Co system, grown on piezoelectric $Pb(Mg_{1/3}Nb_{2/3})_{0.7}Ti_{0.3}O_3$ (110) (PMN-PT) substrates, is achieved at room temperature. Obvious changes in both the coercivity field (H_C) and the exchange bias field (H_E), of 31% and 5%, respectively, have been observed when the electric field is applied to the substrate. While the change of coercivity is related to the enhanced uniaxial anisotropy in the ferromagnetic layer, the change of the exchange bias field can only originate from the spin reorientation in the antiferromagnetic $CoO_{1-\delta}$ layer caused by the strain-induced magnetoelastic effect. A large $H_E/H_C > 2$, and $H_E \sim 110$ Oe at room temperature, as well as the low-energy fabrication of this system, make it a practical system for spintronic device applications.

Keywords: electric control, exchange bias, PMN-PT, magnetic anisotropy

PACS: 85.75.–d, 85.75.Dd, 75.50.–y, 75.30.Gw **DOI:** 10.1088/1674-1056/aba611

1. Introduction

Voltage-controlled magnetism and magnetic properties are crucial for energy-efficient magnetic memories[1] and sensors[2,3] applications. As an important magnetic phenomenon, the exchange bias (EB) effect,[4–7] arising in the exchange-coupled ferromagnetic/antiferromagnetic bilayers, has played a critical role in a range of spintronic devices, such as the giant (or tunneling) magnetoresistance (GMR/TMR) read heads.[8,9] Intense attempts[10–13] on the electric control of EB have been made in the past decade using various materials. However, most of them cannot be applied to the aforementioned devices. The reasons include:

1) In most of those materials, the exchanged bias only exists at a very low temperature. For example, in $YMnO_3$-permalloy bilayers,[10] the EB effect is obtained and controlled at 2 K, far lower than the room temperature.

2) Although the electric control of the EB effect has been reported at room temperature in some systems, such as the system with Cr_2O_3 coupled to Pd–Co multilayers[11] and system with $BiFeO_3$ coupled to $La_{0.7}Sr_{0.3}MnO_3$,[12] the observed EB field (H_E) is very small and even much smaller than the coercivity (H_C). For device applications, the ideal EB system, which contains a ferromagnetic (FM) part at room temperature, would have a high remanent magnetization (M_R) and a coercive field (H_C) lower than the H_E. When $H_E > H_C$, then for a negative H_E, M_R will be positive, independent of any previously applied field. Similarly, for a positive H_E, M_R will always be negative.[14]

3) Usually, the fabrication of such systems, especially for oxide systems, needs to grow thin films at a relatively high temperature, which is not feasible for large-scale thin-film fabrications. For practical applications, we do not need the perfect crystalline structure of the materials but the extraordinary properties and the simplicity of fabrication.

Previously, we have obtained a large EB effect in $CoO_{1-\delta}$/FM systems with an H_E/H_C ratio greater than 2 as well as a blocking temperature beyond the room temperature ($T_B \sim$ 325 K, much higher than the bulk T_N of stoichiometric CoO).[15] Moreover, the $CoO_{1-\delta}$/FM systems can be easily fabricated at room temperature. In this work, isothermal electric control of EB is achieved at room temperature by growing the $CoO_{1-\delta}$/Co films on the top of piezoelectric $Pb(Mg_{1/3}Nb_{2/3})_{0.7}Ti_{0.3}O_3$ (PMN-PT) (110) substrates. A high H_E/H_C ratio up to 1.9 is observed at room temperature, making this system promising for spintronic device applications. High electric field controllability of the EB effect is demonstrated and ascribed to the uniaxial strain induced in the PMN-PT (110) substrates. The significant modulations in the H_C and H_E are ascribed to changes in both the FM anisotropy and the AFM anisotropy in our FM/AFM bilayers, respectively.

*Project supported by the National Key R&D Program of China (Grant Nos. 2017YFA0206303 and 2017YFA020630) and the National Natural Science Foundation of China (Grant Nos. 11975035 and 51731001).

†Corresponding author. E-mail: wurui2010@pku.edu.cn

2. Experiment details

The EB prototype system $CoO_{1-\delta}$/Co bilayers were deposited on the (110)-cut PMN-PT of 0.5 mm thick at room temperature, using pulsed laser deposition (PLD) with a base pressure lower than 3×10^{-8} Torr. Metallic Co and Cu targets of 99.99% purity were used. Before the deposition of $CoO_{1-\delta}$, 3 nm Cu was deposited to suppress the in-plane crystalline and magnetic anisotropy of the top $CoO_{1-\delta}$/Co bilayer. Then, a 40-nm-thick $CoO_{1-\delta}$ film was deposited in the Ar/O_2 mixture atmosphere with oxygen partial pressure of 2.4×10^{-4} Torr at room temperature and followed by the deposition of 3 nm Co at an Ar atmosphere of 1.8×10^{-3} Torr. Finally, a 3-nm-thick Cu capping layer was deposited to protect the sample from the oxidation. The bottom of the PMN-PT substrates was also covered by a 50-nm-thick Cu as the bottom electrode. All depositions were carried out using a laser fluence of ~ 8 J/cm^2 and a repetition rate of 5 Hz. The magnetic properties of the films were measured using the longitudinal magneto-optical Kerr effect (L-MOKE) with a rotatable sample stage. The transmission electron microscope (TEM) images were obtained with a JEOL 2100 field emission electron microscope under 200 kV.

3. Results

Figure 1(a) shows a schematic of the multilayer stack grown on the PMN-PT (110) substrate and a configuration of the circuit for the electric voltage application. From the TEM image shown in Fig. 1(b), we can clearly identify each layer of the film on the PMN-PT substrate. The thicknesses of $CoO_{1-\delta}$ and Co are about 40 nm and 3 nm, respectively. A polycrystalline structure of $CoO_{1-\delta}$ with grain boundaries perpendicular to the substrate is observed in the $CoO_{1-\delta}$ layer, which is induced by the Cu buffer layer.

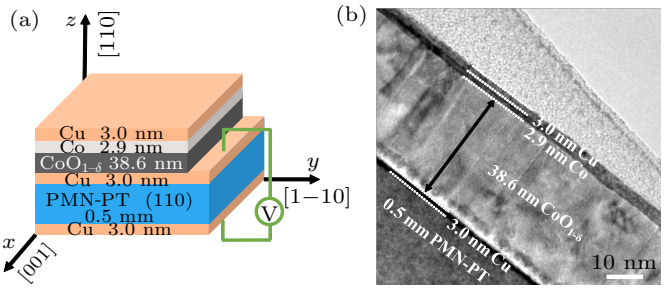

Fig. 1. (a) Schematic of Cu/$CoO_{1-\delta}$/Co/Cu stack grown on PMN-PT(110) substrate and the configuration used for applying an electric field. (b) Cross-sectional TEM image of the stack.

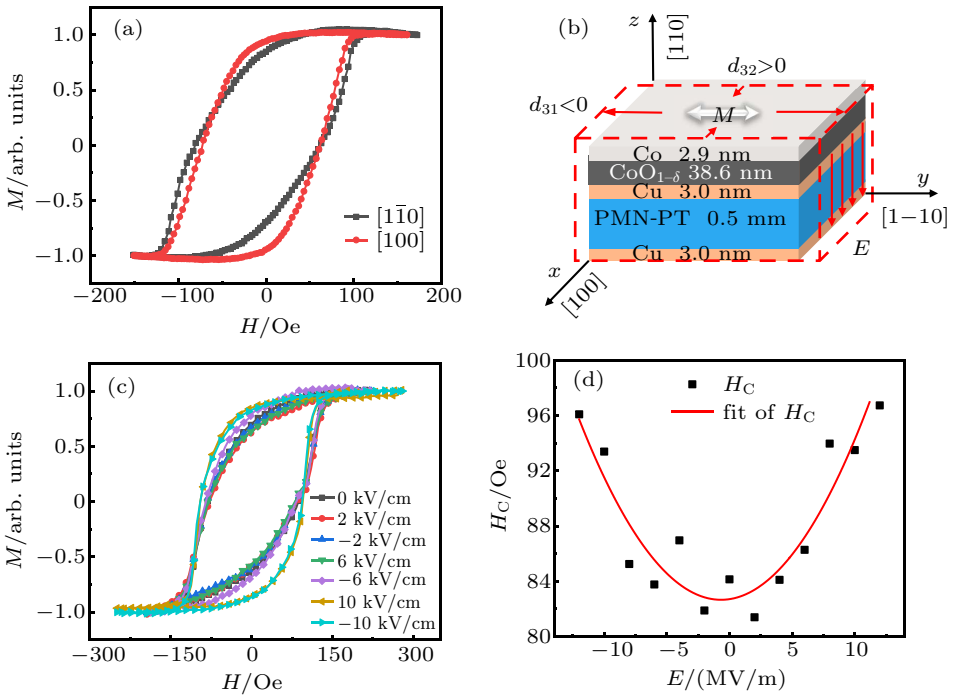

Fig. 2. (a) The ZFC magnetic hysteresis loops measured with magnetic fields applied along the [1−10] and [001] directions. (b) A schematic of the strain induced in the PMN-PT (110) substrate with the applied electric field. (c) The dependence of the ZFC magnetic hysteresis loops along the [1−10] direction upon the applied electric fields. (d) The electric field dependence of the H_C extracted from the hysteresis loops in (c).

First, due to the Cu buffer layer, which has induced a polycrystalline structure in the upper $CoO_{1-\delta}$ layer, there is only a very small in-plane anisotropy of the Co layer, with the [001] direction being the relatively easy axis, as shown in the magnetic hysteresis loops measured with fields applied to the [1−10] and [001] directions (Fig. 2(a)). Then the electric control of the magnetic hysteresis loops along the [1−10] direction was carried out. As shown in Fig. 2(b), a uniaxial strain in PMN-PT (110) substrate with a compressive component in the [001] direction and the tensile component in the [1−10] direction will be induced by the electric fields along the [110] direction, which will be transferred to the $CoO_{1-\delta}$/Co layers via the film–substrate interface. As shown in Fig. 2(c), the hysteresis loops show a strong dependence on the electric field applied

to the substrate, with the H_C and M_R increasing monotonically with the electric field. Meanwhile, the squareness of the hysteresis loop is significantly improved, indicating the enhancement of magnetic anisotropy in the Co layer with the easy axis aligned to the [1−10] direction. This is in good agreement with other studies focusing on Co[16] and CoFeB layers[17,18] grown on PMN-PT (110). The strain dependence of the magnetic hysteresis loops shows a bipolar behavior, which is indicated in the parabolic electric field dependence of H_C shown in Fig. 2(d). In magnetic materials, the spin, orbit, and lattice are strongly coupled to each other, a lattice strain will induce a magnetic anisotropy which could have a dominant effect on the magnetization reversal process. Here, the strain will first affect the electron orbital motion in the top Co layer, and then change the preferred spin orientation via spin–orbit coupling (SOC), which yields a uniaxial magnetic anisotropy and an enhanced coercivity in the easy-axis direction.

To investigate the EB effect of this system, the sample was heated to 330 K and then field cooled (FC) to room temperature with a magnetic field of 500 Oe applied along in-plane [1−10] direction, which was denoted as the 0° direction. After the FC process, the EB effect with a significant shift of about −110 Oe in the hysteresis loop was observed (Fig. 3(a)). With a relatively small $H_C = 60$ Oe, the H_E/H_C ratio is up to ~ 1.9. This makes the $+M_R$ state the only stable state at zero field, which is highly appealing for the application in spintronic devices. With a large $CoO_{1-\delta}$ thickness, the antiferromagnetic spin is stable enough so that there is no observable training effect during a series of magnetic hysteresis loop measurements. This is important for the study of the electric control of the EB. The angular dependence of the hysteresis loop was acquired by rotating the FC sample in the in-plane direction to different angles during the MOKE measurement. Both the H_E and H_C were obtained as functions of the angle. As shown in Fig. 3(b), H_E first undergoes a very slow change with increasing the in-plane angle from 0° to 45°. Then the change becomes faster between 45° and 135°, and finally slows down again between 135° and 180°. In contrast, H_C shows a very sharp decrease at the beginning, slows down between 45° and 135°, and then shows a sharp increase after 135°. Notably, at the angle of 90°, i.e., along the [001] direction, both the H_E and H_C disappear, in contrast with the hysteresis loop measured before the FC. This suggests that, in addition to the induced unidirectional anisotropy in this system, a significant uniaxial anisotropy was also induced during the FC process. This special angular dependence of H_E and H_C can be well explained with the Meiklejohn and Bean (M–B) model shown below,[19,20] which considers both uniaxial and unidirectional anisotropies:

$$\begin{aligned} E = & -J_{FM-AFM} M_{FM} M_{AFM} \cos(\beta - \alpha) \\ & - K_{FM} t_{FM} (\cos(\theta - \alpha))^2 \\ & - K_{AFM} t_{AFM} (\cos(\varphi - \beta))^2 \\ & - H M_{FM} \cos(\alpha) - H M_{AFM} \cos(\beta), \end{aligned} \tag{1}$$

where H and $M_{FM(AFM)}$ are the externally applied magnetic field and the saturation magnetization of the FM (AFM) layer, respectively. $K_{FM(AFM)}$ is the effective uniaxial magnetic anisotropy constant of the FM (AFM) layer, $t_{FM(AFM)}$ is the thicknesses of the FM (AFM) layer, J_{FM-AFM} is the exchange coupling between the FM and AFM layers, while α, β, θ, and φ are the azimuth angles of M_{FM}, M_{AFM}, uniaxial anisotropy axis of FM and uniaxial anisotropy axis of AFM with respect to the applied magnetic field direction, respectively.

As shown in Figs. 3(c) and 3(d), the calculated hysteresis loops and the extracted $H_{E(C)}$ from the M–B model, with parameters of $M_{FM} = 1$, $M_{AFM} = 0.001$, $K_{FM} = 0.5$, $K_{AFM} = 50$, $t_{FM} = t_{AFM} = 1$, $J_{FM-AFM} = 2000$, show a similar angular dependence with the experimental results in Figs. 3(a) and 3(b). However, there are still some discrepancies. For instance, the H_C shows a faster decrease than the experimental data when the angle increases at the beginning, which indicates that this model is oversimplified for the real system. A more accurate approach is given by an empirical formula,[21] which describes the anisotropy field H_A with a series of $\cos(n\varphi)$,

$$H_A(\varphi) = \frac{1}{M} \sum_{n=0} K_n \cos(n\varphi), \tag{2}$$

where M stands for the magnetization, the cosine terms with even n stand for the uniaxial anisotropy and the terms with odd n stand for the unidirectional anisotropy, and K_n stands for the corresponding anisotropy energy. Here in our system, both the uniaxial and unidirectional anisotropies are induced by the FC process. Another key thing to note here is that the H_E/H_C ratio increases to 5 at the angle of 15° while H_E and M_R are nearly unchanged, which further stabilizes the $+M_R$ state.

Then the electric field control of the EB effect was conducted in both the [1−10] and [001] directions, with an electric field applied on the PMN-PT (110) substrate after FC the sample in each direction. First, a positive electric field was applied and increased to 14 kV/cm (corresponding to an electric voltage of 700 V) and magnetic hysteresis loops were measured at every 2 kV/cm with increasing electric field. Then, the electric field was reduced to 0 kV/cm and increased to −14 kV/cm with hysteresis loops measured at every 2 kV/cm again. Figures 4(a) and 4(c) give the hysteresis loops measured at the negative electric fields. The hysteresis loops at positive electric fields show similar behavior. It is observed that, upon the application of the electric field, the squareness of hysteresis loops in the [1−10] direction increases while it decreases in the [001] direction, which is similar to the results obtained with ZFC, as shown in Fig. 2(c). This indicates that, by applying the electric field, a uniaxial magnetic anisotropy is enhanced along the [1−10] direction, which is related to the uniaxial strain of the PMN-PT substrate induced by the electric field.

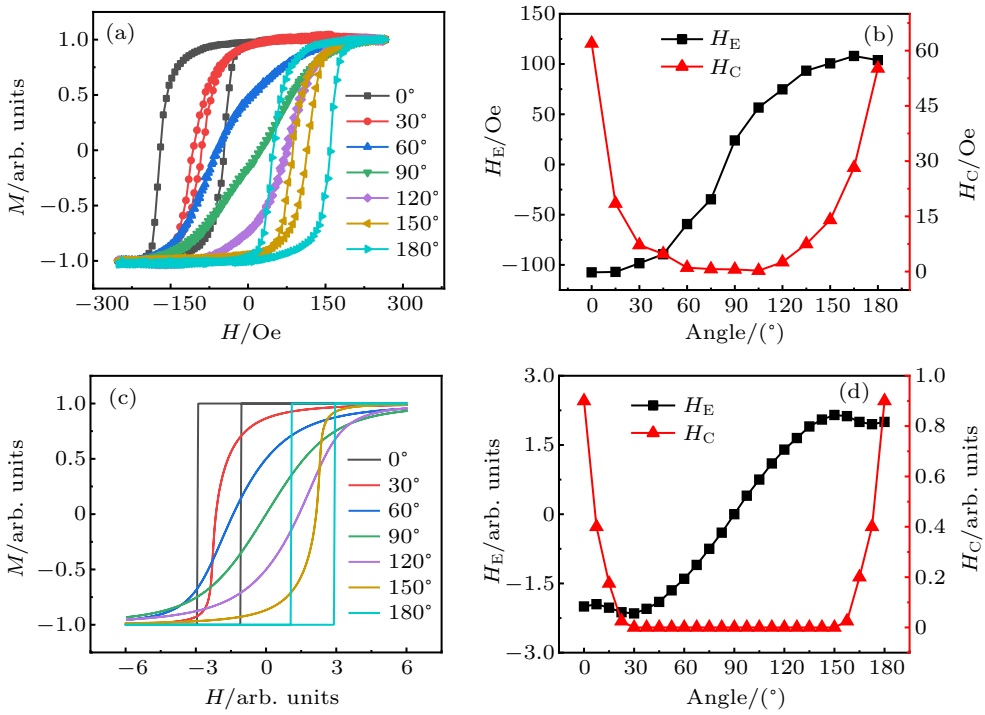

Fig. 3. (a) Angular dependence of hysteresis loops of the $CoO_{1-\delta}$/Co bilayer. (b) The extracted H_E and H_C as functions of the angle. (c) and (d) The angular dependence of the hysteresis loops and the extracted $H_{E(C)}$ calculated with the M–B model.

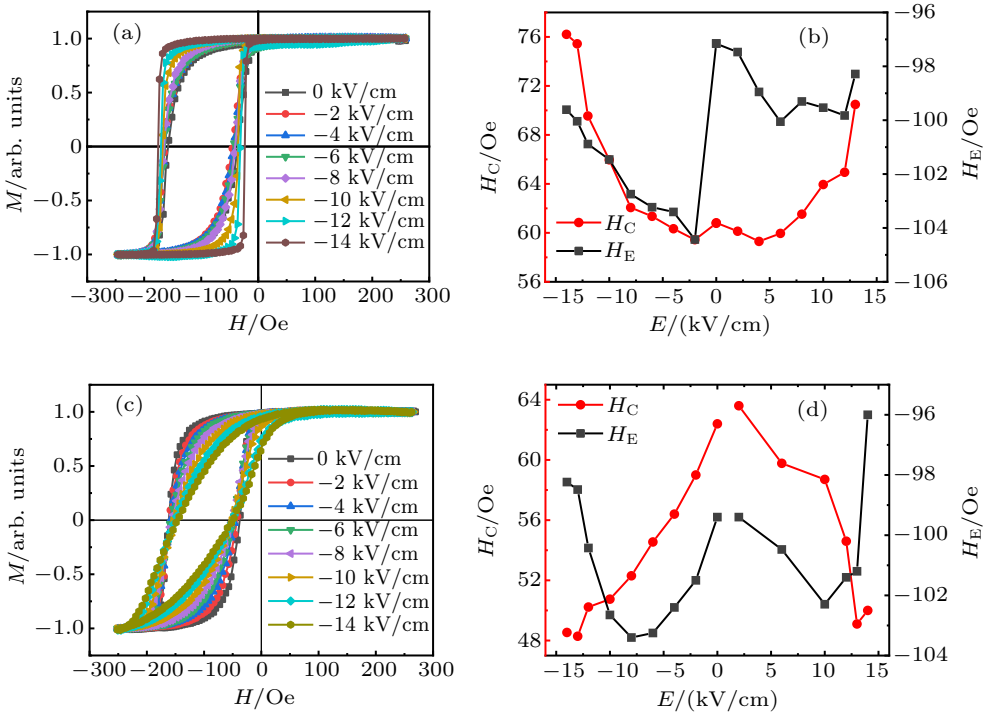

Fig. 4. The voltage dependence of hysteresis loops after the FC procedure along (a), (b) the [1−10] direction and (c), (d) the [001] direction. The hysteresis loops at positive voltages show similar behavior with those at negative voltages.

The H_E and H_C, as the functions of the electric field from 14 kV/cm to −14 kV/cm, are shown in Figs. 4(b) and 4(d) for the [1−10] and [001] directions, respectively. Along the [1−10] direction, the coercivity gradually increases from 58 Oe to 76 Oe with a change of 18 Oe (31%) between 0 kV/cm and −14 kV/cm. However, it shows the opposite trend when the magnetic field is parallel to the [001] axis. It gradually decreases from 64 Oe to 48 Oe with the electric field changing from 0 kV/cm to −14 kV/cm (Fig. 4(d)). A change of nearly 16 Oe (25%) within the electric field range was achieved. The behavior of H_C at the positive electric fields is similar. There is a small asymmetry in the curves under positive and negative electric fields, due to the electrical hysteresis in the substrate caused by the history of the measurements.

Besides the change in the H_C, the H_E also shows a significant change with the electric field. Again, different electric-

field dependences of H_E were observed in these two directions. In the [1−10] direction, the H_E even shows different trends with positive and negative electric fields. With the electric field increasing from 0 kV/cm to −14 kV/cm, the H_E decreases from −104 Oe to −99 Oe, while no obvious change can be observed in the positive directions. Moreover, an obvious step was observed at the point that the electric field changed the polarity. This discontinuity is usually observed in the angular dependence of the EB effect and known as the jump phenomenon.[22] Thus, the similar effect observed here might be related to the relative rotation of the ferromagnetic and the antiferromagnetic anisotropy axes respect to the magnetic field. In the [001] direction, the H_E shows a nonmonotonic dependence on the electric field. In both positive and negative directions, the H_E increases first between 0 kV/cm and ±8 kV/cm and decreases sharply with further increasing the electric field to ±14 kV/cm.

According to the M–B model,[5] the relation $H_E \sim \cos\theta$ can be obtained for the EB systems, where θ is the angle between the magnetic field and the uncompensated AFM net spins at the interface. Hence, the change of H_E with electric fields indicates the rotation of the uncompensated interfacial AFM spins, which is related to the Néel vector of $CoO_{1-\delta}$. This means both the ferromagnetic anisotropy and the antiferromagnetic anisotropy in our system have been manipulated by the voltage-induced strain. However, compared to the strain-induced changes in H_C, the change in H_E is no more than 5%, indicating that the antiferromagnetic anisotropy is more difficult to be tuned than the FM anisotropy in this system, which may be related to a smaller magnetoelastic effect in the $CoO_{1-\delta}$ than that of Co (-9.2×10^7 erg/cm^3).[23–25]

4. Conclusion

The room-temperature electric field tuning of the coercivity and EB field in the $CoO_{1-\delta}$/Co system is realized using the PMN-PT (110) substrates. When the magnetic field is parallel to the [−110] axis, since the axial anisotropy increases as the electric field increases, the coercivity also increases. On the contrary, when the [001] axis of the sample is parallel to the external magnetic field, the electric field increases so that the hysteresis loop is changing from the easy magnetization state to the hard magnetization state, and the coercivity is gradually decreased. The change in the coercivity can be understood with an S–W model, while the behavior of the EB field with applying the electric fields is rather complicated, which has shown a discontinuous change in the [1−10] direction and the nonmonotonic change in the [001] direction. The observed change in H_C and H_E is ascribed to the magnetic anisotropy change induced by the strain in the ferromagnetic and antiferromagnetic layers, respectively, via the magnetoelastic effect. This indicates that the magnetoelastic effect can be utilized in the electric field control of magnetic properties via the exchange coupling. Due to a high H_E/H_C ratio, relatively large H_E, relatively high blocking temperature, and the low fabrication temperature, this system shows prospective applications in electric field controllable spintronic devices.

References

[1] Newhouse-illige T, Liu Y, Xu M, Reifsnyder Hickey D, Kundu A, Almasi H, Bi C, Wang X, Freeland J W, Keavney D J, Sun C J, Xu Y H, Rosales M, Cheng X M, Zhang S, Mkhoyan K A and Wang W G 2017 *Nat. Commun.* **8** 15232

[2] Xiang L, Yu G, Hao W, Ong P V, Wong K, Qi H, Ebrahimi F, Upadhyaya P, Akyol M, Kioussis N, Han X, Amiri P K and Wang K L 2015 *Appl. Phys. Lett.* **107** 142403.1

[3] Zhang L, Wing S and Leung C M 2015 *J. Appl. Phys.* **117** 17A748

[4] Kiwi M 2001 *J. Magn. Magn. Mater.* **234** 584

[5] Meiklejohn W H and Bean C P 1957 *Phys. Rev.* **105** 904

[6] Wu R, Ding S, Lai Y, Tian G and Yang J 2018 *Phys. Rev. B* **97** 024428

[7] Wu R, Xue M, Maity T, Peng Y, Giri S K, Tian G, MacManus-Driscoll J L and Yang J 2020 *Phys. Rev. B* **101** 014425

[8] Gan H D, Matsukura F, Miura K, Ikeda S, Mizunuma K, Ohno H, Hayakawa J, Yamamoto H, Kanai S and Endo M 2010 *Nat. Mater.* **9** 721

[9] Miron I M, Garello K, Gaudin G, Zermatten P J , Costache M V, Auffret S, Bandiera S, Rodmacq B, Schuhl A and Gambardella P 2011 *Nature* **476** 189

[10] Martí X, Sánchez F, Hrabovsky D, Fàbrega L, Ruyter A, Fontcuberta J, Laukhin V, Skumryev V, García-Cuenca M V, Ferrater C, Varela M, Vilà A, Lüders U and Bobo J F 2006 *Appl. Phys. Lett.* **89** 32510

[11] He X, Wang Y, Wu N, Caruso A, Vescovo E, Belashchenko K, A Dowben P and ChristianBinek 2010 *Nat. Mater.* **9** 579

[12] Wu S M, Cybart S A, Yu P, Rossell M D, Zhang J X, Ramesh R and Dynes R C 2010 *Nat. Mater.* **9** 756

[13] Wu S M, Cybart S A, Yi D, Parker J M, Ramesh R and Dynes R C 2013 *Phys. Rev. Lett.* **110** 067202

[14] Choi E M , Weal E, Bi Z, Wang H, Kursumovic A, Fix T, Blamire M G and MacManus-Driscoll J L 2013 *Appl. Phys. Lett.* **102** 012905

[15] Ding S L, Wu R, Fu J B, Wen X, Du H L, Liu S Q, Han J Z, Yang Y C, Wang C S, Zhou D and Yang J B 2015 *Appl. Phys. Lett.* **107** 172404

[16] Rizwan S, Ali S I, Zhang Q T, Zhang S, Zhao Y G, Anis-Ur-Rehman M, Tufail M and Han X F 2013 *J. Appl. Phys.* **114** 104108.1

[17] Wu S Z, Miao J, Xu X G, Yan W, Reeve R, Zhang X H and Jiang Y 2015 *Sci. Rep.* **5** 8905

[18] Rizwan S, Yu G Q, Zhang S, Zhao Y G and Han X F 2012 *J. Appl. Phys.* **112** 064120

[19] Meiklejohn W H 1962 *J. Appl. Phys.* **33** 1328

[20] Xia Y H, Wu R, Zhang Y F, Liu S Q, Du H L, Han J Z, Wang C S, Chen X P, Xie L, Yang Y C and Yang J B 2017 *Phys. Rev. B* **96** 064440

[21] Wu X, Ambrose T and Chien C 1998 *Appl. Phys. Lett.* **72** 2176

[22] Bai Y, Yun G and Bai N 2010 *J. Appl. Phys.* **107** 033905

[23] Sander D 1999 *Rep. Prog. Phys.* **62** 809

[24] Valeri S, Altieri S and Luches P 2010 *Magnetic Properties of Antiferromagnetic Oxide Materials: Surfaces, Interfaces, and Thin Films* (Weinheim: Wiley-VCH Verlag GmbH & Co. KGaA) pp. 25–68

[25] Chen Y T, Jen S U, Yao Y D, Wu J M, Lee C C and Sun A C 2006 *IEEE Transactions on Magnetics* **42** 278